

# Journal of Materials Chemistry A

Accepted Manuscript



This is an *Accepted Manuscript*, which has been through the Royal Society of Chemistry peer review process and has been accepted for publication.

*Accepted Manuscripts* are published online shortly after acceptance, before technical editing, formatting and proof reading. Using this free service, authors can make their results available to the community, in citable form, before we publish the edited article. We will replace this *Accepted Manuscript* with the edited and formatted *Advance Article* as soon as it is available.

You can find more information about *Accepted Manuscripts* in the [Information for Authors](#).

Please note that technical editing may introduce minor changes to the text and/or graphics, which may alter content. The journal's standard [Terms & Conditions](#) and the [Ethical guidelines](#) still apply. In no event shall the Royal Society of Chemistry be held responsible for any errors or omissions in this *Accepted Manuscript* or any consequences arising from the use of any information it contains.

## Large area, flexible polyaniline/buckypaper composite with core-shell structure for efficient supercapacitors

*Shaoqing He, Jinquan Wei<sup>\*</sup>, Fengmei Guo, Ruiqiao Xu, Can Li, Xian Cui, Hongwei Zhu, Kunlin Wang, Dehai Wu*

Key Lab for Advanced Materials Processing Technology of Education Ministry; State Key Lab of New Ceramic and Fine Processing; School of Materials Science and Engineering, Tsinghua University, Beijing 100084, P. R. China

\*Corresponding author: jqwei@tsinghua.edu.cn

### Abstract

We fabricated efficient polyaniline (PANI)/buckypaper supercapacitors based on continuous growth of flexible carbon nanotube (CNT) film and electro-deposition technique. The PANI/buckypaper electrodes have core-shell structure which reduce internal resistance and enhance charge transfer between PANI and CNT bundles. The performance of supercapacitors depend on the content and morphology of PANI. The PANI/buckypaper supercapacitors show high specific capacitance of ~430 F/g with high energy density of ~140 Wh/kg and high power density of ~200 kW/kg when the PANI content is about 70 wt.%.

## 1. Introduction

Supercapacitor, consisting mainly of porous electrode, electrolyte and separator, is an attractive energy storage device bridging the gap between conventional capacitors and rechargeable batteries in energy density. The porous electrode holds the key for achieving high efficient supercapacitor, which is required to have high capacitance, stability, low resistance, ease of obtain, environmental-friendly, and sometime flexibility<sup>1,2</sup>. Carbon nanotubes (CNTs) are promising candidates to serve as supercapacitor electrode due to their high conductivity, low density, and large specific surface area<sup>3-8</sup>. Recently, there are considerable attempts to use CNTs as electrodes to enhance the capacitance of supercapacitors<sup>9-18</sup>. The specific capacitance were enhanced significantly by pretreating the CNTs, such as functionalization, activation, and heat-treatment<sup>3, 9-12</sup>. CNTs incorporated with metallic oxide or polymers were also proposed to improve the specific capacitance of the supercapacitors<sup>13-18</sup>, where oxide/polymer increase the capacitance value by providing extra pseudocapacitance. Flexible CNT supercapacitors based on conducting polymer composite, such as polypyrrole (PPy), polyaniline (PANI) are also reported<sup>19-24</sup>.

As one of conventional conductive polymers, PANI has been actively investigated in supercapacitor due to its high pseudocapacitance, low cost and ease of fabrication. Various types of carbon nanotubes, including single-walled, double-walled, multi-walled CNTs (SWCNTs, DWCNTs, MWCNTs), aligned CNT arrays, paper-like film, have been used in supercapacitors incorporated with PANI<sup>17, 18, 22-29</sup>. These research demonstrated not only the potential applications of the CNTs but also the influence of CNTs' characters on the performance of supercapacitors. Generally, the specific capacitance of the supercapacitors made from macroscopic CNTs are superior to those from CNT powders due to lower internal resistance. Core-shell structure of polymer/CNTs can shorten charge transfer path between polymer and CNTs, which can reduce the internal resistance and enhance the capacitance. Niu et al. report a "skeleton/skin" supercapacitor from SWCNT/PANI composite, showing an optimized specific capacitance of 236 F/g and high energy density of 131 Wh/kg<sup>28</sup>.

Here, we report an efficient supercapacitor using PANI/buckypaper composite with CNT-core and PANI-shell structure as electrode based on continuous growth of CNT films and electro-deposition process. The PANI/buckypaper supercapacitor behaves high performances benefit from both good PANI/CNTs interface and low internal resistance.

## 2. Experimental

### Fabrication of buckypaper

Large area CNT films were prepared continuously by using a floating catalyst CVD method which is similar to our previous reports<sup>30</sup>. Xylene solution containing ~0.4 M ferrocene and 0.02 M sulfur were atomized by an ultrasonic sprayer and sent into a quartz tube reactor by H<sub>2</sub>/Ar carrier gas. The reaction temperature was set to 1150 °C. CNTs grow very fast and form continuously unwoven films. The CNT films were carried out by gas flow and collected by a spool at a speed of ~5 m/min. The CNT films peeled from the spool were loose, flexible and hydrophobic. The as-grown CNT films were immersed into ethanol solution and then shrank into densely packed buckypaper after drying.

### Fabrication of PANI/buckypaper composite

The PANI/buckypaper composites were fabricated by electro-deposition method in an aqueous electrolyte of 0.1 M aniline and 1M H<sub>2</sub>SO<sub>4</sub> at a scan rate of 50 mV/s, where the buckypaper, platinum electrode and saturated Calomel electrode (SCE) were used as working electrode, counter electrode and reference electrode, respectively<sup>17</sup>. The aniline monomer accumulates on the CNT bundles and polymerize under effect of current. The content of PANI in the PANI/buckypaper composites was controlled by the scanning cycles. After polymerization, the PANI/buckypaper composite was washed with 0.5 M H<sub>2</sub>SO<sub>4</sub>, and then cleaned with de-ionized water for several times to remove the residual aniline and H<sub>2</sub>SO<sub>4</sub>. Finally, the composites are dried in a vacuum oven at 80 °C for 12 h.

## Characterization

The supercapacitors were fabricated by separating two PANI/buckypaper films with a microspore membrane in 0.5M H<sub>2</sub>SO<sub>4</sub> aqueous solution electrolyte. The electrochemical performances of the supercapacitors were measured by two-electrode method using a chemical station (CHI 660D, CHI Instruments). The PANI/buckypaper composites were characterized and evaluated by using scanning electron microscopy (SEM, LEO-1530), transmission electron microscopy (TEM, JEOL-2011), Raman spectroscopy (Renishaw System 2000), and X-ray photoelectron spectroscopy analysis (XPS, PHI-5300ESCA), respectively.

## 3. Results and discussion

Large area CNT films are grown continuously by the floating CVD method at a speed of above 300 m/h (see video in supporting materials). Fig. 1a shows an optical image of the CNT films with width of ~6 cm peeled from a spool. By infiltrating with ethanol, the loose CNT films densely packed into buckypaper. Fig. 1b shows an optical image of a buckypaper with dimension of 18 cm × 4 cm. The buckypapers are flexible and easy to be folded or rolled into various shapes. Inset of Fig. 1b demonstrates a buckypaper roll with diameter of about 1 cm. Fig. 1c is a cross-sectional SEM image of a buckypaper with thickness of ~20 μm. The buckypaper consists of hundreds of layer of CNT films.

Fig. 1d presents a SEM image of the CNT film. There are very low amount of amorphous carbon and catalyst particles in the CNT films, showing high purity of CNT films. The film consists of ultra-long CNTs due to rapid growth. It is hard to observe CNT tips during SEM examination. The nanotubes in the film are mainly SWCNT and DWCNT according to TEM examination and Raman spectra (see Fig. 1e and 1f). The Raman spectrum shows very low D band (1320 cm<sup>-1</sup>) and high G-band (1587 cm<sup>-1</sup>). The intensity ratio of G-band to D-band of the as-grown film is about  $I_G/I_D=25$ , showing low defect density in the CNTs. Several radial breathing mode

(RBM) peaks located at 135, 156, 191, 198, 214, 250, and 280  $\text{cm}^{-1}$  are identified, corresponding to SWCNTs and DWCNTs with diameters varied from  $\sim 0.7$  to  $\sim 2$  nm. Due to consisting of ultra-long SWCNTs and DWCNTs with low defect density, the buckypapers are highly conductive. The sheet resistance of is only about 5  $\Omega/\text{sq}$ .

The PANI is coated on the CNT bundles by electro-deposition method at a scan rate of 50 mV/s from -1 V to 1 V in aqueous solution with 0.1 M aniline and 1M  $\text{H}_2\text{SO}_4$ , which forms PANI/buckypaper composites. Aniline monomers polymerize on the CNT bundles stimulated by current due to good affinity with CNTs. SEM images of the composites obtained. Fig. 2 shows SEM images of the PANI/buckypaper obtained from various deposition cycles, which reveal the morphology evolution of the composite. At the low deposition cycle of 2 (Fig. 2a), aniline begin to polymerize and distribute on the CNT bundles. The diameters of CNT bundles increase slightly when compare with those of the as-grown samples. The morphology of the composite also differs from that of the as-grown buckypaper (see Fig. 1d). As the deposition cycle increases, it forms continuous PANI layer coating on the CNTs bundles (Fig. 2b and 2c). The diameter of the PANI/CNT also increases. The PANI nanofibers separate out and deposit on the PANI/buckypaper composite when the deposition cycle is higher than 24 (see Fig. 2d). After that, the PANI nanofibers cover on the PANI/buckypaper composite gradually. Fig. 2e shows a SEM image of the composite covered completely by nanofibers. The PANI nanofibers are  $\sim 300$  nm in diameters and several microns in length. Fig. 2f demonstrates a SEM image of the composite after partially removing the PANI nanofibers. It is clear that the morphology of PANI/buckypaper composite underneath the PANI nanofibers is similar to those prepared at deposition cycle of 24. The content of PANI in the composite is calculated by the weight gain after removing the residual solution by washing with de-ionic water several times followed by freeze dehydration at  $-50$   $^\circ\text{C}$  for long time ( $>48$  hours). The composites shown in Fig. 2a to 2e, corresponding to deposition cycles of 4, 8, 16, 24 and 32, contain about 19 wt.%, 46 wt.%, 60 wt.%, 71 wt.%, and 83 wt.% PANI, respectively.

TEM images clearly reveal the polymerization of PANI on the CNT bundles in

more details. The PANI begins to deposit on but not surround the CNT bundles for 2 cycle deposition (Fig. 3a). After 4 deposition cycle, the PANI surround the CNT bundles and form disconnecting thin film (Fig. 3b). When the deposition cycle reaches to 16, the PANI layers surround the CNT bundles continuously. It forms PANI/CNT core-shell nanocomposite, which is similar to those depositing on CNT powder<sup>17</sup>. Fig. 3d shows a high resolution TEM image of a CNT bundle coated with PANI layer. As shown by circles in Fig. 3d, partial crystalline PANI on the CNT bundle are identified, indicating good interface between PANI and CNTs.

Fig. 4 shows Raman spectra of the PANI/buckypaper composites with different content of PANI. The Raman peaks centered at  $210\text{ cm}^{-1}$  and  $1590\text{ cm}^{-1}$  correspond to RBM and G-band of the CNTs, while the peaks centered at  $412\text{ cm}^{-1}$ ,  $576\text{ cm}^{-1}$ ,  $1165\text{ cm}^{-1}$  and  $1485\text{ cm}^{-1}$  contribute from the PANI<sup>31</sup>. The peaks at  $210\text{ cm}^{-1}$  and  $1590\text{ cm}^{-1}$  decreases as the content of PANI increases, indicating good interaction between the CNT bundles and PANI.

The electrochemical characterization of the PANI/buckypapers are measured by two-electrode method in 0.5 M aqueous  $\text{H}_2\text{SO}_4$  electrolyte. We use the weight of PANI/buckypaper to calculate the specific capacitance for all the capacitors. Fig. 5a shows a set of CV curves of the composite containing 71 wt.% PANI at different scan rates varied from 10 mV/s to 500 mV/s. The CV curves have good rectangle shape, even at high scan rate of 500 mV/s, showing nearly ideal double-layer capacitors of the PANI/buckypaper. The specific capacitance of the 71 wt.% PANI/buckypaper at low scan rate of 5 mV/s reaches to 430 F/g, which is more than 20 times higher than that of the pure buckypaper (18 F/g), also higher than that of SWCNT/PANI (236 F/g) reported recently<sup>28</sup>. The specific capacitances of the PANI/buckypaper decrease only about 20% when the scan rate increases from 5 mV/s to 500 mV/s, showing potential applications in fast charge-discharge process. Fig. 5b depicts the profiles of voltage versus time obtained by the galvanostatic charge-discharge technique at various current densities. The charge-discharge curves show good symmetry in the potential range, indicating that the supercapacitor has a high reversibility between charge and discharge processes.

A Nyquist plot of the 71 wt.% PANI/buckypaper supercapacitor is shown in Fig. 5c. The plot has an almost ideally vertical curve in the low frequency, indicating good capacitive behavior of the device. The plot does not show semicircle region (see inset of Fig. 5c), probably because of the low internal resistance of the composite. The internal resistance of the capacitor is only  $\sim 0.7 \Omega$  according to the impedance spectrum, which is lower than that of the pure buckypaper sample ( $\sim 0.9 \Omega$ ). The low internal resistance derives from efficient charge transfer between PANI shell and SWCNT bundle core.

We measured the stability of the PANI/buckypaper capacitor by galvanostatic charge-discharge test at a high current density of 10 A/g. Fig. 5d shows a plot of specific capacitance versus testing cycle for the 71 wt.% PANI/buckypaper supercapacitor. The specific capacitance lost about 15% after 500 charge-discharge cycles, and  $\sim 20\%$  (from 430 F/g to 340 F/g) after 1000 charge-discharge cycles. The stability of the PANI/buckypaper supercapacitor is much better than that of pure PANI nanofiber capacitor. The loss of capacitance derives from instability of PANI during long-term charge-discharge cycling 32.

The specific capacitance of the PANI/buckypaper supercapacitors are affected by the content of PANI in the composite. Fig. 6a shows the CV curves of the supercapacitors using different PANI/buckypapers as electrodes at a scan rate of 200 mV/s. The calculated specific capacitance is about 18 F/g, 160 F/g, 214 F/g, 253 F/g, 352 F/g and 295 F/g for the pure buckypaper and PANI/buckypaper with 19 wt.%, 46 wt.%, 60 wt.%, 71 wt.% and 83 wt.% PANI, respectively. The specific capacitance of the composite increase initially as the content of PANI increase, resulting from forming PANI/buckypaper core-shell structure. As the content of PANI exceeds 71 wt.%, the specific capacitance of the supercapacitor begin to decrease due to separation of PANI nanofibers on the PANI/buckypaper composite. The charge transfer in pure PANI is much harder than in PANI/buckypaper. The galvanostatic charge-discharge curves obtained by using a current density of 10 A/g also shows the trend of specific capacitance depending on the content of PANI (see Fig. 6b). Fig. 6c demonstrates the dependence of specific capacitance on the scan rate for the

supercapacitors with different content of PANI. The specific capacitance increases from 18 F/g to 427 F/g when the PANI content increases from 0 to 71 wt.%, while it decreases from 427 F/g to 362 F/g when the content of PANI increases from 71 wt.% to 83 wt.%.

As an energy storage device, supercapacitor bridges the gap of conventional capacitors and lithium-ion batteries in energy density. The maximum energy density is given by  $W_{\max}=CV^2/2$ , where V is the applied voltage. The energy density of the PANI/buckypaper varies from ~60 Wh/kg to 140 Wh/kg, which is higher than recent report (131 Wh/kg)<sup>28</sup> and close to that of the conventional lithium-ion battery<sup>33</sup>. The maximum power density ( $P_{\max}=V^2/4mR_i$ , where  $R_i$  is the internal resistance, m is the total mass of two electrodes.) increases as the scan rate and capacitance of the PANI/buckypaper. The maximum power density is about 200 kW/kg for the PANI/buckypaper with 71 wt.% PANI at a scan rate of 500 mV/s (see Fig. 6d).

#### 4. Conclusions

We demonstrated that PANI/buckypaper with CNT-core and PANI-shell structure are promising electrode materials for efficient supercapacitors based on continuous CNT growth process and electro-deposition approach. The content of PANI in the composite is well controlled by the electro-deposition cycle. The performances of the supercapacitors depend on the content of PANI significantly. The PANI/buckypaper supercapacitor with 71 wt.% PANI shows high specific capacitance of ~430 F/g, high power density of 200 kW/kg, and high energy density of ~140 Wh/kg. The core-shell PANI/CNT facilitates charge transfer and reduces the internal resistance. The continuous fabrication approach of the flexible CNT films in high quality make it possible to construct high performance flexible supercapacitors for various applications.

## Acknowledgements

This work was supported by Natural Science Foundation of China (51172122), Beijing Specific Nanoscience and Nanotechnology Project (Z121100001312002), Tsinghua University Initiative Scientific Research Program (20111080939), Cooperation Project of Beijing Nova Program (XXHZ201204).

## References

1. L. Nyholm, G. Nystrom, A. Mihranyan and M. Stromme, *Adv. Mater.*, 2011, 23, 3751.
2. M. Armand, and J.M. Tarascon, *Nature*, 2008, 451, 652.
3. C. M. Niu, E. K. Sichel, R. Hoch, D. Moy and H. Tennent, *Appl. Phys. Lett.*, 1997, 70, 1480.
4. K. H. An, W. S. Kim, Y. S. Park, J. M. Moon, D. J. Bae, S. C. Lim, Y. S. Lee and Y. H. Lee, *Adv. Funct. Mater.*, 2001, 11, 387.
5. H. Pan, J. Y. Li and Y. P. Feng, *Nanoscale Res. Lett.*, 2010, 5, 654.
6. J. H. Chen, W. Z. Li, D. Z. Wang, S. X. Yang, J. G. Wen and Z. F. Ren, *Carbon*, 2002, 40, 1193.
7. E. Frackowiak, *Phys. Chem. Chem. Phys.*, 2007, 9, 1774.
8. D. N. Futaba, K. Hata, T. Yamada, T. Hiraoka, Y. Hayamizu, Y. Kakudate, O. Tanaike, H. Hatori, M. Yumura and S. Iijima, *Nat. Mater.*, 2006, 5, 987.
9. K. H. An, W. S. Kim, Y. S. Park, J. M. Moon, D. J. Bae, S. C. Lim, Y. S. Lee and Y. H. Lee, *Adv. Funct. Mater.*, 2001, 11, 387.
10. X. Zhao, B. T. T. Chu, B. Ballesteros, W. L. Wang, C Johnston, J. M. Sykes and P. S. Grant, *Nanotechnology*, 2009, 20, 065605.
11. E. Frackowiak, S. Delpeux, K. Jurewicz, K. Szostak, D. Cazorla-Amoros and F. Beguin, *Chem. Phys. Lett.*, 2002, 361, 35.
12. P. L. Taberna, G. Chevallier, P. Simon, D. Plee and T. Aubert, *Mater. Res. Bull.*, 2006, 41, 478.
13. I. H. Kim, J. H. Kim, Y. H. Lee and K. B. Kim, *J. Electrochem. Soc.*, 2005, 152, A2170.
14. A. L. M. Reddy, M. M. Shaijumon, S. R. Gowda and P. M. Ajayan, *J. Phys. Chem. C*, 2010, 114, 658.
15. S. Jagannathan, T. Liu and S. Kumar, *Compos. Sci. Technol.*, 2010, 70, 593.
16. J. Wang, Y. L. Xu, X. Chen and X. F. Sun, *Compos. Sci. Technol.*, 2007, 67, 2981.
17. V. Gupta and N. Miura, *Electrochim. Acta*, 2006, 52, 1721.

18. C. Z. Meng, C. H. Liu, L. Z. Chen, C. H. Hu and S. S. Fan, *Nano Lett.*, 2010, 10, 4025.
19. G. Nystrom, A. Razaq, M. Stromme, L. Nyholm, and A. Mihranyan, *Nano Lett.*, 2009, 9, 3635.
20. L. Nyholm, G. Nystrom, A. Mihranyan, and M. Stromme, *Adv. Mater.*, 2011, 23, 3751.
21. A. Razaq, L. Nyholm, M. Sjodin, M. Stromme, and A. Mihranyan, *Adv. Energy Mater.*, 2012, 2, 445.
22. Z. B. Cai, L. Li, J. Ren, L. B. Qiu, H. J. Lin, and H. S. Peng, *J Mater. Chem. A*, 2013, 1, 258.
23. J. Ren, L. Li, C. Chen, X. L. Chen, Z. B. Cai, L. B. Qiu, Y. G. Wang, X. R. Zhu, and H. S. Peng, *Adv. Mater.*, 2013, 25, 1155.
24. J. Ren, W. Y. Bai, G. Z. Guan, Y. Zhang, and H. S. Peng, *Adv. Mater.*, 2013, 25, 5965.
25. C. Z. Meng, C. H. Liu and S. S. Fan, *Electrochem. Commun.*, 2009, 11, 186.
26. H. Zhang, G. P. Cao, W. K. Wang, K. G. Yuan, B. Xu, W. F. Zhang, J. Cheng and Y. S. Yang, *Electrochim. Acta*, 2009, 54, 1153.
27. Y. Zhou, Z. Y. Qin, L. Li, Y. Zhang, Y. L. Wei, L. F. Wang and M. F. Zhu, *Electrochim. Acta*, 2010, 55, 3904.
28. Z. Q. Niu, P. S. Luan, Q. Shao, H. B. Dong, J. Z. Li, J. Chen, D. Zhao, L. Cai, W. Y. Zhou, X. D. Chen and SS Xie, *Energ. Environ. Sci.*, 2012, 5, 8726.
29. H. J. Lin, L. Li, J. Ren, Z. B. Cai, L. B. Qiu, Z. B. Yang and H. S. Peng, *Sci. Rep.*, 2013, 3.
30. J. Q. Wei, B. Jiang, D. H. Wu and B. Q. Wei, *J. Phys. Chem. B*, 2004, 108, 8844.
31. G. M. do Nascimento and M. L. A. Temperini, *J Raman Spectroscopy*, 2008, 39, 772.
32. S. R. Sivakkumar, W. J. Kim, J. A. Choi, D. R. MacFarlane, M. Forsyth, and D. W. Kim, *J Power Sources*, 2007, 171, 1062.
33. J. M. Tarascon and M. Armand, *Nature*, 2001, 414, 359.

## Figures

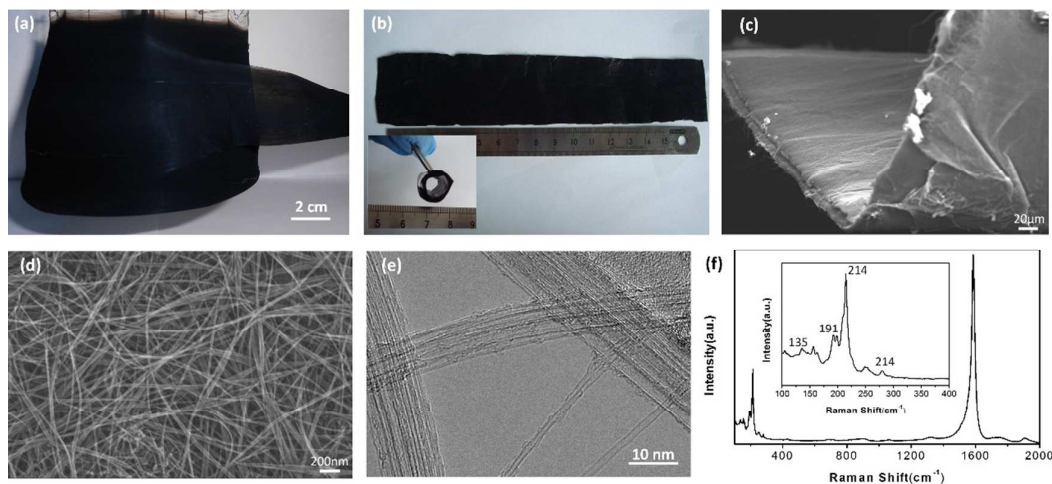


**Fig. 1.** Characterization of the CNTs using in experiments. (a) Macroscopic image of CNT films peeled off from a spool. (b) A buckypaper with dimension of 18 cm  $\times$  4 cm. Inset: The buckypapers are flexible and can be easily rolled into a cylinder. (c) Side-viewed SEM image reveals the multilayer structure of the buckypaper. (d) High magnification SEM image. (e) TEM image. (f) Raman spectrum. Inset, radial breathing mode.

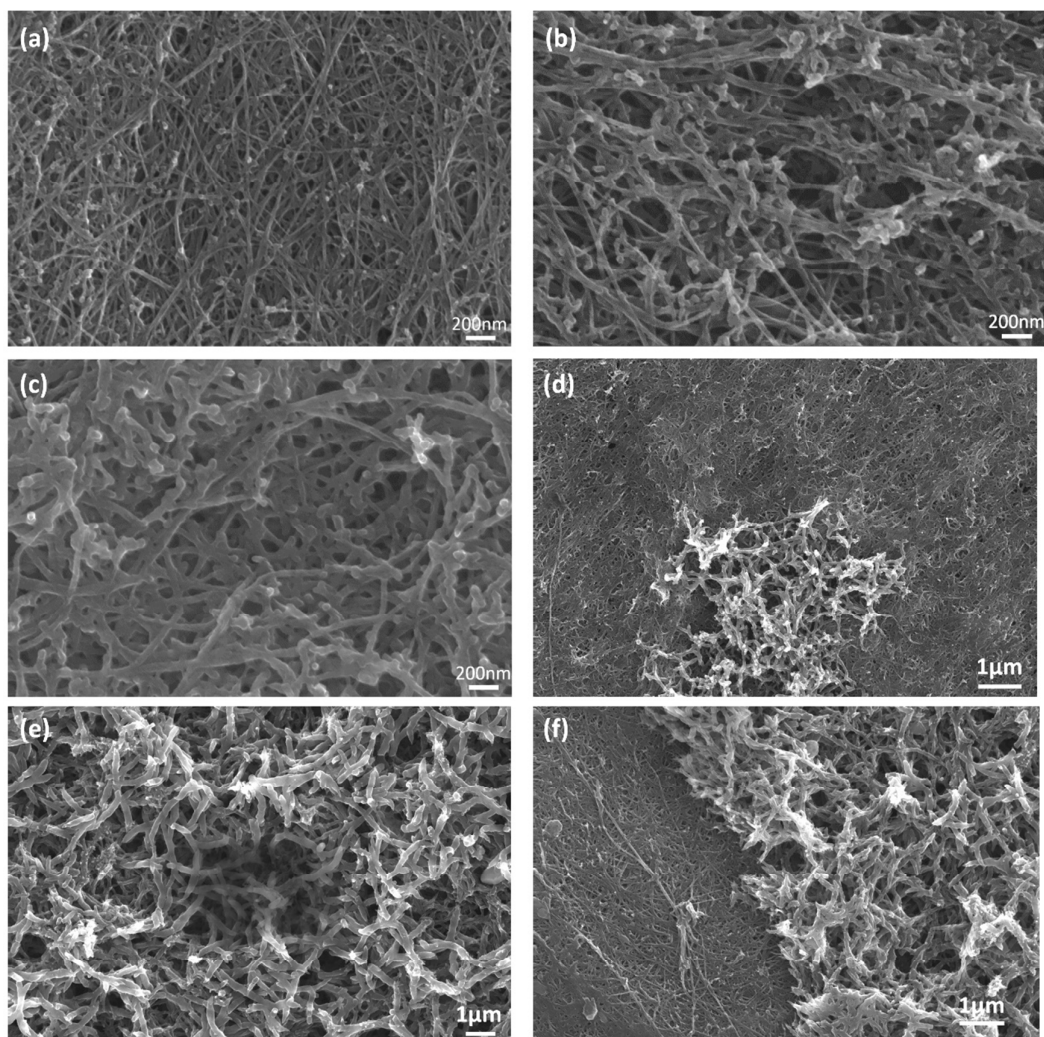


**Fig. 2** SEM image of the PANI/buckypaper composite prepared by (a) 4 (b) 8 (c) 16 (d) 24 (e) 32 electro-deposition cycles. (f) After partial removal of PANI nanofibers from the composite prepared by 32 electro-deposition cycles.

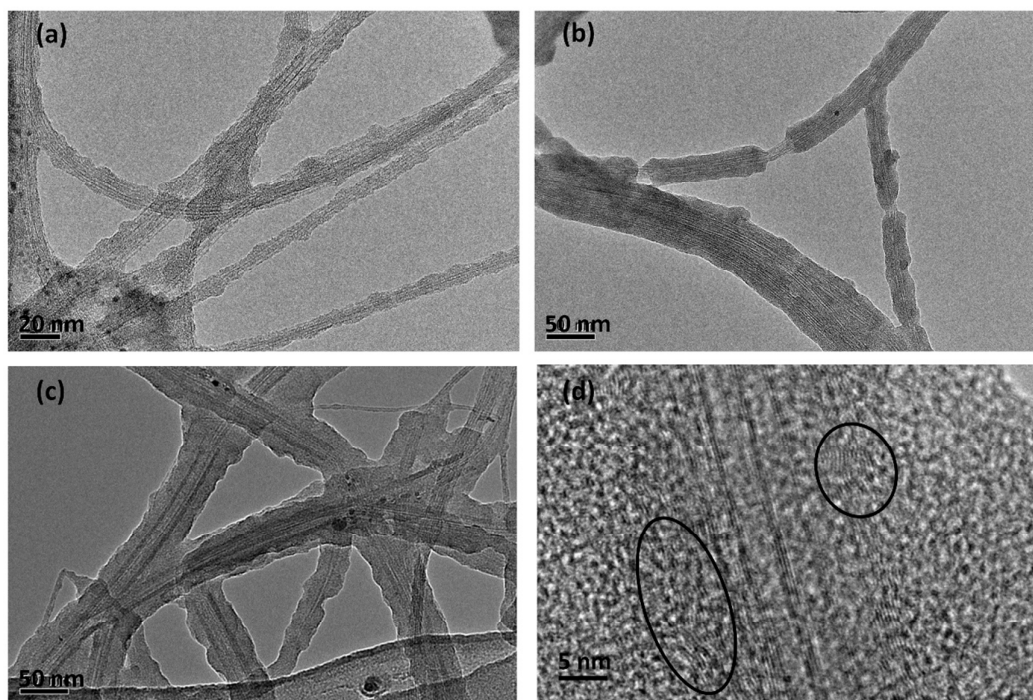


**Fig. 3** TEM images of the PANI/buckypaper with various percentage of PANI. (a) 19 wt.%, (b) 46 wt.%, (c) 60 wt.%, (d) High resolution TEM image of a CNT bundle coated by PANI.

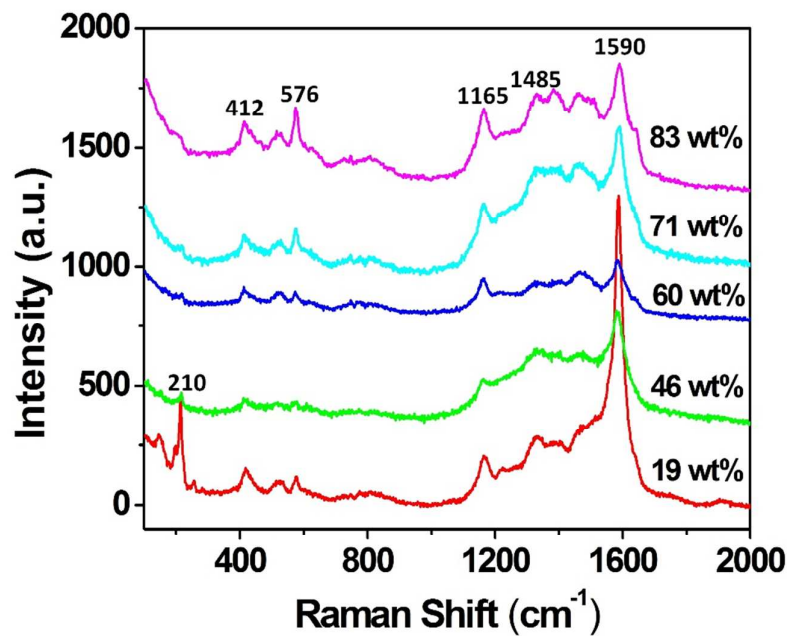


**Fig. 4** Raman spectra of the PANI/buckypaper composites with different content of PANI.

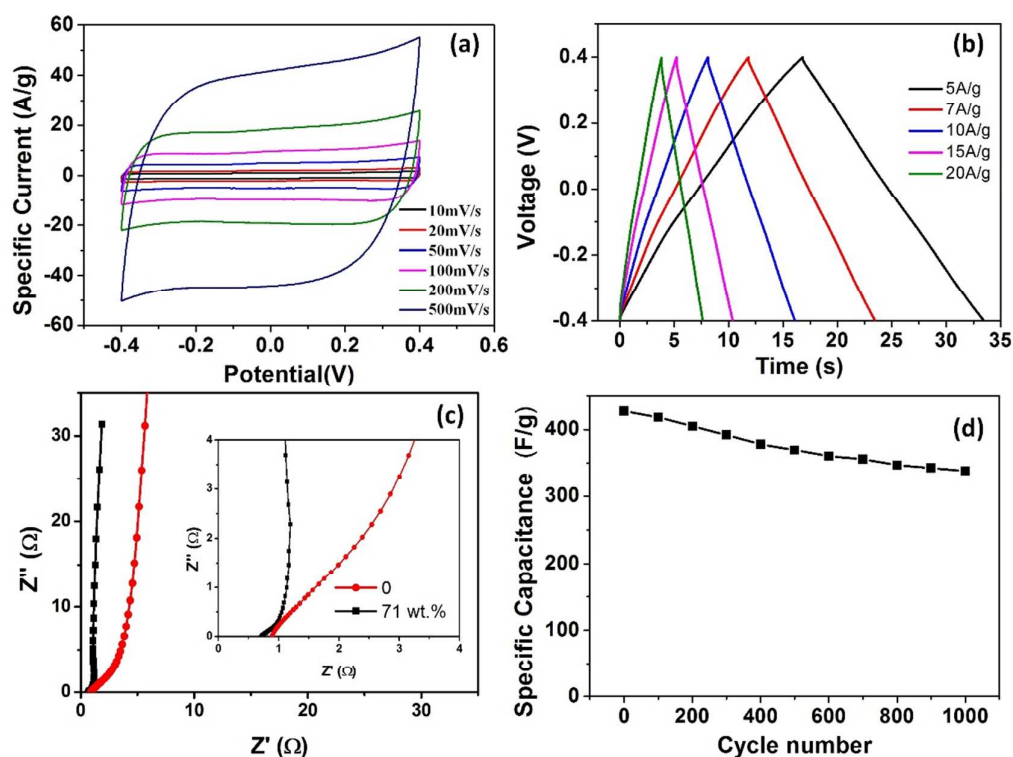


**Fig. 5.** Supercapacitor performance of the 71 wt.% PANI/buckypaper composite. (a) CV curves measured at different scan rates. (b) Galvanostatic charge-discharge curves under different constant current densities. (c). Impedance plot,  $Z'$ : real impedance,  $Z''$ : imaginary impedances. Inset: The enlarged plot shows no evident Nyquist semi-circle. A Nyquist plot of pure buckypaper is also provided. (d). Charge-discharge cycling stability of a PANI/buckypaper composite supercapacitor.

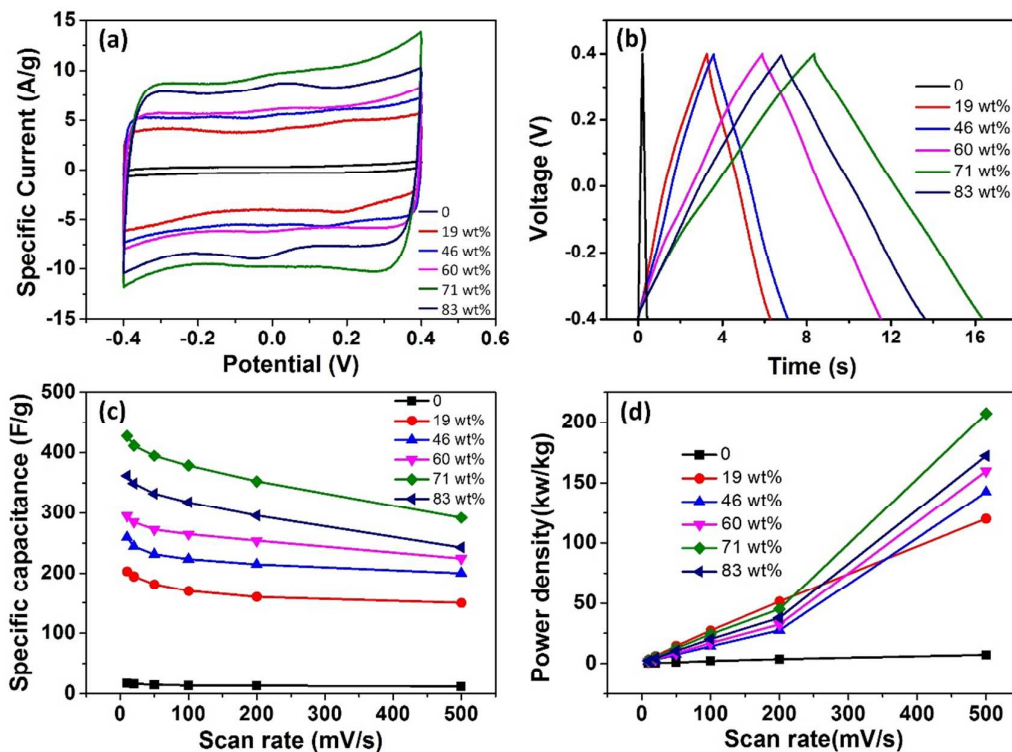


**Fig. 6.** Supercapacitor performance PANI/buckypaper composites with different content of PANI. (a) CV curves measured at a scan rate of 100 mV/s. (b) Galvanostatic charge-discharge curves measured at 10 A/g. (c). Calculated specific capacitances of the PANI/SWCNT supercapacitors at various scan rates. (d) Power density of the PANI/buckypaper supercapacitors at various scan rates.

## Supporting Materials

Video of continuous growth of CNT films.